Title: A requirement for correctly scaled synapses in the regulation of motor circuit output

Authors: Tanya Zubov, Lara do Amaral-Silva, Joseph M. Santin*

*Email for correspondence: jmsantin@uncg.edu

Affiliations: [1]The University of North Carolina at Greensboro, Department of Biology

Keywords: homeostatic plasticity, synaptic scaling, AMPA receptor, compensation, control of breathing

Abstract

Synaptic scaling is a compensation mechanism that adjusts all synapses by the same relative amount to regulate neuronal activity. However, synaptic compensation does not always scale uniformly, leaving to question if a scaling rule is required to regulate circuit output. We previously showed that scaling up excitatory synapses on motoneurons regulates the respiratory network following inactivity caused by hibernation in frogs (Santin et al., 2017). Although synaptic scaling is thought to involve a scaling factor that multiplicatively upregulates synaptic strength, we find here that distinct mechanisms account for the upregulation of mean synaptic strength and the scaling organization. These processes are separable, as blocking L-type Ca^{2+} channels undoes the scaling pattern of compensation but does not interfere with the mean increase in synaptic drive. Strikingly, motor output from the respiratory network was weaker when motoneuron synapses were “unscaled” despite having the same average amount of compensation after hibernation. Thus, parallel mechanisms regulate the amount and organizational pattern of synaptic scaling, and both must work appropriately for proper network function. Collectively, these results emphasize that an apparently normal amount of synaptic compensation may still lead to circuit dysfunction in neurological disorders if the balance of synaptic inputs is not accurately regulated.

Introduction

Neural circuits must produce the correct output patterns to generate reliable behaviors. However, animals face constantly changing internal and external environments, posing a threat to stable neuronal function (1). To maintain stability, the nervous system is thought to use a wide range of homeostatic mechanisms that sense activity perturbations which then modify cellular and synaptic function to regulate neuronal output. Mounting evidence now indicates these processes act during physiological conditions such as development (2, 3), sleep (4), hibernation (5), and associative learning (6), while inappropriate function of homeostatic mechanisms may lead to various neurological disorders (7-10).

Although diverse homeostatic mechanisms exist (11, 12), the most well-studied involves compensatory changes in excitatory synaptic strength through a mechanism termed synaptic scaling. Synaptic scaling is classically interpreted to involve the up or downregulation of all a neuron's synaptic inputs by the same relative amount to oppose activity disturbances by uniformly scaling postsynaptic neurotransmitter receptors (13). For example, if neuronal activity drops, the function of AMPA-glutamate receptors double at every synapse to counteract reduced firing rates. Although a large body of work supports cell-wide multiplicative synaptic scaling (2, 5, 6, 13-16), activity perturbations can induce non-uniform and synapse-specific modifications (17-21), leaving to question the advantage of precise synaptic scaling for the function of neural networks. On the one hand, multiplicative scaling of synaptic weights will maintain the balance of synaptic inputs across the neuron, and altering this balance has been suggested to cause information loss at synapses (22). On the other, inducing

compensation only at select synapses has been proposed to improve information transfer (21) and stability of networks with complex architectures (20, 23). Whether biological networks rely on a scaling rule to generate appropriate outputs, and the network-level consequences of failing to scale synaptic compensation, remains to be determined.

We have been using the respiratory network of hibernating American bullfrogs, *Lithobates catesbeianus*, to address how stable network function arises in response to an physiologically-relevant activity perturbation (24). Lung ventilation is normally a vital neuromotor behavior. However, during under water hibernation, gas exchange demands are met through cutaneous respiration, and the motor circuits that produce lung breathing stop entirely. After months of inactivity, frogs emerge in the spring and quickly display normal respiratory motor performance (25, 26). We previously found that respiratory motoneurons scale up AMPA-glutamate receptor currents in response to aquatic hibernation which serves to maintain respiratory motor outflow immediately after the network restarts (5). Given that hibernation causes a large and chronic reduction in neuronal output, these results suggest that inactivity during winter triggers synaptic scaling for the regulation of motor performance in the spring (5, 24). To isolate the role of inactivity from other environmental feedback (*e.g.*, cold temperature), we aimed to determine if tetrodotoxin (TTX), a common tool used to block network activity in studies of synaptic compensation, also causes synaptic scaling in this system. Despite similar average increases in total postsynaptic strength by hibernation and TTX, we found that only hibernation showed evidence of multiplicative synaptic scaling. Thus, we took advantage of this system to understand the differential control of synaptic strength and

regulation of the balance of synaptic inputs. This positioned us to then address the longstanding question of how disrupting the correct balance of synaptic weights during compensation impacts network performance.

Results

Motoneurons that innervate the glottal dilator in American bullfrogs (4th branch vagal motoneurons; Fig. 1A) undergo compensatory upregulation of AMPA-glutamate receptor currents in response to ~2 months of aquatic hibernation (5). To simulate the overwintering environment in this study, frogs were cooled from 20°C to 2°C over one week and then held at 2°C for either two or four weeks before assessing synaptic strength in brain slices. Consistent with our previous report with inactivity at longer time scales, synaptic strength, as assessed by the amplitude of spontaneous excitatory postsynaptic currents (sEPSC; no TTX), increased in frogs exposed to the simulated hibernation environment at both two and four weeks (Supp Fig. 1A) with no change in sEPSC frequency (Supp Fig. 1A, $p=0.182$; one-way ANOVA). These results confirm postsynaptic compensation in response to hibernation and demonstrate that upregulation of excitatory synaptic strength plateaus at a new steady-state value relatively early into aquatic submergence.

Many reports indicate that variables associated with inactivity (*i.e.*, loss of postsynaptic firing or synaptic transmission) can drive homeostatic increases in synaptic strength (27, 28). Our rationale was that if synaptic compensation during winter is responding to inactivity, pharmacological inactivity may produce a similar degree and pattern of compensation as hibernation. To test this, we silenced intact respiratory networks in the brainstem-spinal cord preparation with 100 nM TTX for 16 hours. While the time courses of hibernation (one month) and shorter-term TTX (16 hours) are clearly different, synaptic scaling has been observed to manifest rapidly after 4 hours of inactivity in vitro (27). This allowed us, as a first approximation, to isolate the role of

network inactivity in inducing synaptic scaling in the absence of the winter environment. We compared average miniature excitatory postsynaptic current amplitude in slices (mESPCs) following TTX to Time Controls (control preparations with rhythmic activity present for 16 hrs at 22°C) and Post-Hibernation preparations (preparations recovered following hibernation for 16 hrs at 22°C). TTX and hibernation groups exhibited similar mean increases in cell-averaged mEPSC amplitude relative to Time Control preparations. These mean increases were not different from each other (Fig. 1C-D). Increased amplitude following TTX and hibernation was not associated with changes in passive membrane properties, mEPSC frequency, and mEPSC decay tau (Supp Fig. 2). Therefore, short-term pharmacological inactivity produces a similar average amount of synaptic compensation as long-term physiological inactivity.

Given that the entire mEPSC amplitude distribution is thought to be regulated by a scaling factor(s) during inactivity (22), we next determined whether the increase in postsynaptic strength following TTX and Hibernation occurred similarly across the distribution of individual mEPSCs. Despite similar distributions between control and TTX groups, the shape of these distributions diverged above the 75th%ile of mEPSC amplitudes and below the 40th%ile (Fig. 1D and inset). Thus, the distribution shape between TTX and Post-Hibernation were significantly different (Kolmogorov-Smirnov test; $p=0.02$). Collectively, these results indicate that inactivity by TTX and Hibernation lead to differences in the shape of the mESPC distribution despite similar mean changes in synaptic drive.

The Komogorov-Smirnov test is highly sensitive to changes in the shape of distributions and, therefore, may be prone to false positives with a large sample sizes

(29). Therefore, we next determined whether the difference identified between TTX and post-hibernation mEPSC distributions fell within the range of variability in our system (false positive) or whether this slight difference was, indeed, a true positive. First, we compared the mEPSC distributions between two distinct control groups to determine the data set-to-data set variability in the mEPSC distributions. When comparing mESPC distributions from two control groups, they were statistically indistinguishable (Supp. Fig. 3A; p=0.55). Second, we exposed a second Post-Hibernation group to TTX to silence activity during the 16 hr incubation period. This allowed us to determine if TTX and hibernation distributions subtly differed (Fig. 1D) because hibernation induces a distinct synaptic response or because the presence of rhythmic activity after hibernation *in vitro* modifies the distribution of synaptic weights. Mean mEPSC amplitude was similar in post-hibernation and post-hibernation preparations exposed to TTX (Supp. Fig. 3B; p=0.367), and the amplitude distributions were well-matched (Supp. Fig. 3C and inset; p=0.51, Kolmogorov-Smirnov test). Therefore, these additional experiments provide evidence that inactivity during hibernation upregulates the mEPSC amplitude through a different distribution compared to short-term inactivity with TTX.

Given that TTX and hibernation upregulated synaptic strength but had different distributions, we wanted to determine if both showed evidence of multiplicative scaling. We used the rank-order method to test for synaptic scaling of mESPC amplitudes in populations of neurons (6, 13, 30). To do this, an equal number of mEPSCs from control and inactive cells were rank-ordered from the smallest to largest amplitude, plotted against each other (ranked control vs. ranked treatment), and fit with a linear regression (Supp Fig. 4). The treatment distribution for each form of inactivity was then

mathematically downscaled by the equation of the line, and the scaled distribution was compared to control. If synaptic scaling occurs, there should be a statistically indistinguishable matching between the scaled and control distributions of mEPSC amplitudes.

As expected, all forms of inactivity strongly increased the amplitude distribution of mEPSCs relative to control (Fig. 2A-C; K-S test; time control vs. all treatment conditions; $p<0.0001$). When we performed the downscaling transformation on the TTX distribution, interestingly, the control and scaled TTX distributions did not precisely overlap (Fig. 2A; $p=0.002$). Although these two distributions are similar, close inspection shows separation throughout most of the bottom 30-40%ile (Fig 2A inset). In contrast, the mathematically downscaled post-hibernation (Fig. 2B and inset) and post-hibernation+TTX (Fig. 2C and inset) distributions matched the control distributions, producing p values of 0.624 and 0.712, respectively (K-S test). These results indicate that hibernation upregulates synaptic drive while maintaining the balance of synaptic weights, indicative of synaptic scaling, but TTX does not.

These results suggest that mechanisms controlling the upregulation of postsynaptic strength, and how the mEPSC distribution is organized, may be controlled independently. To accomplish either of these tasks, we hypothesized that Ca^{2+} may play a role, as it is well known to control diverse aspects of neuronal plasticity and function. For example, loss of Ca^{2+} influx through L-type Ca^{2+} channels during inactivity can drive synaptic scaling up (27), and L-type Ca^{2+} channels also organize AMPA receptors at excitatory synapses (31). Therefore, we addressed the role of L-type Ca^{2+} in controlling total synaptic strength, the organization of the mEPSC amplitude distribution, or both

following hibernation. To address this, we exposed rhythmic circuit preparations to 10 µM nimodipine, a blocker of L-type Ca^{2+} channels in motoneurons of this system (32), for 16 hours in warm-acclimated preparations and following synaptic scaling in post-hibernation period. Exposure of warm-acclimated preparations to nimodipine did not affect mean mEPSC amplitude or the distribution relative to warm-acclimated time control (Fig. 3A-C). In addition, post-hibernation preparations exposed to nimodipine still resulted in upregulation of cell-averaged mEPSCs compared to time controls (Fig 3A-B), just as we observed with TTX, post-hibernation, and post-hibernation+TTX (Fig. 1, Supp. Fig. 3). Thus, reduced L-type channel function does not drive compensation in this system, and Ca^{2+} feedback through L-type channels does not maintain cell-averaged synaptic strength in its compensated state.

We then assessed whether post-hibernation networks exposed to nimodipine still exhibited evidence of synaptic scaling. Interestingly, when using warm-acclimated time controls and warm-acclimated preparations treated with nimodipine as reference points for scaling, we no longer found evidence of multiplicative scaling of the mEPSC distribution when post-hibernation preparations were treated with nimodipine (Fig. 3C-D). Close inspection of the cumulative distributions reveals a poor matching of the downscaled and control distributions below the 50%ile (Fig.3C-D and insets). When comparing the distribution of synaptic events in the post-hibernation+nimodipine group to post-hibernation alone (scaling intact), the upper 50th%ile of the mEPSC distributions appeared to separate (K-S test; $p=0.02$), while cell-averaged synaptic mEPSC amplitude were not different ($p=0.470$, Fig. 3E). These results indicate that Ca^{2+} signaling through L-type channels organizes the mEPSC distribution independently from

the average amount of compensation. Consequently, nimodipine treatment “undoes” apparent multiplicative scaling by subtly reducing synaptic strength of the upper half of the distribution (Fig. 3). Altogether, our data provide evidence that inactivity triggers persistent increases in total synaptic drive and independent factors associated with calcium signaling maintains the balance of synaptic inputs following hibernation.

The previous experiments set the stage for us to assess motor circuit function when synapses have been upregulated and scaled (post-hibernation; Fig. 2B) or when scaling has been disrupted (post-hibernation+nimodipine; Fig. 3C-D). The respiratory network is a central pattern generating network, which permits the recording of respiratory-related motoneuron firing *ex vivo* (Fig. 4A). In this preparation, extracellular population motor burst frequency of the cut nerve root provides information regarding the function of the rhythm generating networks (33), and integrated burst shape relates to motoneuron firing and/or recruitment (34). Across controls (time control and warm-acclimated+nimodpine), scaled-compensated (post-hibernation), and unscaled-compensated groups (post-hibernation+nimodipine), no differences existed in frequency of the respiratory rhythm at 13 hrs *in vitro* (Supp Figure 5A). However, preparations with motoneuron synapses “unscaled” had shorter motor burst widths relative to control preparations and those where compensation remained appropriately scaled (Fig. 4 B-C). In addition, nimodipine application to warm-acclimated preparations did not affect burst width, showing that burst narrowing by nimodipine was specific to networks following hibernation. In support of a slow disruption of synaptic scaling after hibernation to reduce motor outflow, acute application of nimodipine did not affect burst width in any group (Fig. 4C), indicating that short term changes in network excitability by nimodipine

do not account for burst narrowing. Furthermore, intrinsic membrane properties of motoneurons did not appear to differ across groups (Supp Figure 5B-F) which rules out other obvious neurophysiological properties that could reduce the population motor burst. Altogether, these experiments suggest that synaptic compensation must be scaled correctly to produce normal network function associated with breathing.

Discussion

Synaptic scaling implies that a multiplicative scaling factor up or downregulates the efficacy of synapses equally in response to activity disturbances. Instead of a single scaling factor that drives up synaptic strength, we found that the organization of scaling can be controlled independently from the average amount of compensation. Furthermore, when we “unscaled” multiplicative scaling, dysfunctional network activity followed. Our data add support for the view that similar average compensatory responses may be organized in different ways (35), corroborating studies which highlight that multiple combinations of channels and receptors can generate similar neuronal outputs (36, 37). However, different solutions for the same degree of compensation do not have identical outcomes on circuit behavior, and some may drive undesirable network states for the animal as we describe here.

Separable mechanisms control synaptic compensation and the quantitative organization of synaptic scaling

An important finding of this study is that separable mechanisms regulate total synaptic drive and quantitative scaling of individual synaptic weights. Three lines of evidence led us to this conclusion:

First, inactivity associated with hibernation and TTX increased synaptic strength through distinct mEPSC distributions despite similar mean amounts of compensation (Fig. 1C-D). We acknowledge that this difference was subtle, but when we performed a set of additional experiments to block activity with TTX after hibernation (Supplemental Fig. 3C-D), both hibernation distributions were statistically indistinguishable. In addition, mEPSC distributions from distinct control groups were also the same. These results

indicate that the mEPSC distribution in this system is largely stable, hibernation consistently shifts the distribution of individual synaptic events, and the scaling organization persists regardless of whether activity is present following hibernation (Supp. Fig. 3). Therefore, similar increases in mean mEPSC amplitude are achieved by differentially modifying the mEPSC distribution depending on whether inactivity is induced by short term TTX or physiological inactivity during hibernation.

Second, when we performed the standard rank-order test for multiplicative scaling (6, 13, 16), hibernation but not TTX showed evidence of multiplicative synaptic scaling (Fig. 3). In line with these results, TTX applied to the hippocampus *in vivo* drives up synaptic strength without evidence of scaling as determined by the rank-order method (19). A recent study also suggested that TTX may not lead to uniform scaling in different mammalian neuronal types when assessed using the rank-order method (18), although there is significant evidence to the contrary (14, 27, 29, 38). Unlike TTX, hibernation led to evidence of multiplicative scaling. While we used the standard method to draw this conclusion, we acknowledge the need to note recent studies suggesting that every synapse may not be regulated at the same multiplicative level. Specifically, synaptic spine density and AMPAR expression across individual synapses do not scale uniformly within the same neuron even though multiplicative scaling appears to occur at the population level (21, 39). A non-zero y-intercept in the linear model used to test for scaling may also suggest additive processes work alongside multiplicative scaling mechanisms (29). In contrast, the y-intercept has been interpreted to compensate for mEPSCs that fall below the detection cutoff and is, therefore, needed to align control and scaled distributions to demonstrate multiplicative scaling (13, 40). In support of the

later possibility, the y-intercept values we obtained for both linear models in the two hibernation groups were sufficient to compensate for our 7pA cutoff within <0.1pA (Supp Fig. 4). Future work must assess whether physiological evidence of synaptic scaling in different contexts, systems, and transformation methods reflects uniform changes in AMPAR receptor expression or a more complicated strategy that involves diverse postsynaptic adjustments (*e.g.*, receptor expression, post-translation modification), as well as presynaptic changes across synapses.

The previous results do not indicate whether scaling and upregulation are independently controlled or whether TTX and hibernation induce different forms of synaptic compensation. Our data show that upregulation of synaptic strength can be uncoupled from the scaling organization by inhibiting L-type Ca^{2+} channels, indicating that each are controlled by separate mechanisms in this system. Blocking L-type Ca^{2+} channels before hibernation did not affect mEPSC properties and the amplitude distribution. These results differ from traditional models of synaptic compensation/scaling in neuronal cultures, whereby reduced Ca^{2+} influx through L-type channels led to upregulated synaptic strength (17, 27, 41, 42). Thus, inactivity-sensitive processes are likely to upregulate synaptic strength in this system without a contribution from L-type channels (Fig. 1). In contrast, the block of L-type Ca^{2+} channels *following* winter inactivity disrupted the scaling organization without influencing the mean amount of compensation. These results indicate that Ca^{2+} feedback is a signal for the correct synaptic distribution after the network has turned back on following hibernation (Fig. 3), and these mechanisms persist even without ongoing activity (Supp. Fig. 3C). Although these results may appear contradictory, spontaneous neurotransmitter release can lead

to subthreshold activation of L-type channels on dendrites to induce neuronal plasticity (43, 44). Furthermore, as cold temperature increases membrane input resistance (45, 46), spontaneous neurotransmitter release may cause larger postsynaptic depolarizations compared to warm animals, generating significant Ca^{2+} influx through L-type channels to orchestrate scaling of compensation. Therefore, we speculate that activation of L-type channels at subthreshold voltages during hibernation may provide a signal for induction of the scaling organization, which then requires ongoing calcium influx, either during network activity or when the network is silent, to maintain it. Taken together, synaptic upscaling does not reflect a single scaling factor that globally increases synaptic strength, but rather, separate processes: one that increases mean synaptic strength and at least one other that accurately organizes scaling through signaling that involves L-type Ca^{2+} channels.

Synaptic organization influences network function despite similar synaptic drive

Our previous study identified that synaptic scaling likely acts at respiratory synapses to maintain motor output associated breathing following hibernation (5). Those experiments involved low-dose block of AMPARs to reduce the number of functional AMPARs in the network and showed a greater sensitivity of the respiratory motor outflow to inhibition after hibernation. In the present study, we effectively performed the inverse experiment and disrupted the scaling organization on the motoneuron while leaving the overall enhancement of synaptic drive intact.

Our results argue for a requirement of scaled synaptic weights to maintain respiratory motor function. We draw this conclusion because population motor output was reduced when synaptic strength of motoneurons was upregulated but not correctly

scaled after hibernation (Fig. 4). Given that output from this motor nerve activates musculature that permits airflow into the lung (47), accurate synaptic scaling is likely needed to regulate lung ventilation following winter inactivity. We recognize the challenge of attributing changes in high-level network properties to subtle shifts in the distribution of synaptic weights on motoneurons, and we made several attempts to address other variables that could explain these results. First, rhythmic burst frequency of the network was the same across all groups after 13 hr *ex vivo*; thus, overall activity differences and altered rhythm generator function is unlikely to explain shorter motor bursts. Second, several intrinsic and network properties did not change (Supp Fig. 5). Third, exposing warm-acclimated control preparations to nimodipine before hibernation did not affect the amplitude distribution of mEPSC, motor burst width, or any other obvious electrophysiological property, arguing against other actions of nimodipine on different parts of the network (Fig. 3B, Supp. Fig. 5). Finally, acute exposure to nimodipine did not affect burst duration in any group (Fig. 4D), suggesting that slow disruption of Ca^{2+} feedback after hibernation alters synaptic organization that shapes burst duration rather than acute effects of calcium channel blockade on network excitability. Altogether, these results, in concert with our previous findings (5), strongly imply that the correct balance of upregulated synaptic weights contributes to the maintenance of network homeostasis follow perturbation.

How does altering the scaling organization of the same average compensation lead to changes in motor function? Mechanistically, we speculate this may occur if respiratory synapses are not evenly scaled relative to non-respiratory synapses, such as those involved in vocalization (48). Our data are consistent with this possibility. Fig.

4E shows that the upper 50^{h}%ile of post-hibernation preparations treated with nimodipine appear to be slightly reduced compared to post-hibernation alone. If these synapses are responsible for breathing, their weakening may result in a failure to sustain motoneuron firing, shortening respiratory burst duration. Given that the specific synapses for respiratory motor output are not yet known, future work must aim to understand how a failure to scale motoneurons synapses translates to altered respiratory-driven firing responses at the single neuron level, and also how other network properties may change to necessitate motoneuron scaling for network output (24). Nevertheless, our observations support a role for the precise scaling of individual synaptic weights to maintain network behavior.

General Implications

Synaptic scaling of postsynaptic AMPA receptor currents is a well-documented compensatory response to reduced activity across diverse neurons and systems. Whether synaptic scaling is important for network function remained unknown. Using a system that uniquely allowed us to uncouple mean upregulation of synaptic strength from scaling of the mEPSC distribution, our results lead us to suggest that comparable amounts of synaptic compensation can produce network dysfunction if the distribution of synaptic weights is not correctly scaled. Proper synaptic scaling has clear adaptive value following hibernation, as it ensures adequate motor drive for lung ventilation (1; present study Fig. 5). More broadly, our results demonstrate that “homeostatic” synaptic plasticity could lead to pathological circuit output if neurons do not correctly organize synaptic weights. In this view, accurate compensation at the cell-level could be “anti-homeostatic” for network function if the incorrect synaptic organization is left unchecked.

We acknowledge this conclusion is most applicable to feedforward networks, as networks with complex architectures including combinations feedforward and feedback excitation may use different compensation strategies to maintain stable outputs (23). Along these lines, many neurological disorders are thought to involve a failure of homeostatic synaptic mechanisms (7). Yet, in some cases aberrant network states emerge despite seemingly normal ability to compensate through changes in the strength of excitatory synapses. For example, upregulation of excitatory synapses during inactivity remains intact in certain cell types in models of Fragile X syndrome (49, 50) and Rett syndrome (51). Although neurological disorders are clearly multifactorial, we suggest that pathological network states could arise not only from inappropriate amounts of total compensation (too much or too little), but also from a failure to engage mechanisms that correctly organize seemingly normal amounts of compensation across synapses. If distinct mechanisms for regulating the amount and organization of synaptic compensation occurs in other systems, attention must then be directed towards understanding the potentially diverse processes that ensure compensation remains well-organized to achieve stable network output.

Materials and Methods

Animals

Bullfrogs of either sex weighing approximately 100 g were purchased from the Rana Ranch (Twin Falls, ID, USA). Control frogs were maintained at 20 ºC in plastic tubs and were provided aerated water with access to wet and dry areas. Frogs were fed pellets provided by Rana Ranch once per week. Hibernation conditions were simulated in temperature controlled incubators. The temperature of water was lowered from 20ºC to 2ºC over the course of a week, dropping about 2-3 degrees per day. On the seventh day, a plastic screen was placed at the top of the water to block to prevent access to the surface. Animals do not eat at cold temperatures; therefore, food was also withheld while frogs remained at 2°C. All frogs in each condition were kept on a 12 hr:12 hr light: dark cycle. Experiments were only performed during the light cycle.

Dissection and Tissue Preparation

Brainstem-spinal cord dissections were performed as previously described (5). Briefly, frogs were deeply anesthetized with approximately 1 ml of isoflurane per liter and rapidly decapitated. The head was immersed in chilled bullfrog artificial cerebrospinal fluid (aCSF) and the brainstem-spinal cord was removed, keeping the motor rootlets of the vagus intact (aCSF; concentrations in [mM]: 104 NaCl, 4 KCl, 1.4 $MgCl_2$, 7.5 glucose, 40 $NaHCO_3$, 2.5 $CaCl_2$ and 1 NaH_2PO_4, and gassed with 98.5% O_2, 1.3%CO_2; pH = 7.85). Following the dissection, the brain was superfused with aCSF with a flow rate of ~6 mL per minute.

To selectively label laryngeal branch motoneurons that innervate the glottal dilator, the 4th branch of the vagus nerve was isolated and then backfilled tetramethylrhodamine dextran 3000 MW (Life Technologies Corporation, Eugene, OR USA). Approximately 1 uL of 10% dextran was loaded into the tip of a glass pipette that fit snuggly around the cut 4th root of the vagus, as this nerve contains axons that most innervate the glottal dilator, a respiratory muscle in anuran amphibians (see references provided in 5). Backfills lasted two hours and produced robustly labeled neurons for electrophysiological recording. Following the dye loading process, tissue was sliced with a vibratome at 300 µM. Sections approximately 300-600 µm rostral to the obex were used for electrophysiological recording. Tissue slices were left to recover for an hour before electrophysiological recording.

Whole-cell patch clamp recordings

Slices containing labeled motoneurons were transferred to recording chamber, stabilized with a nylon grid, and exposed to aCSF at a flow rate of ~1-2 mL per min supplied via a gravity-fed system. The region containing labeled neurons was imaged at 4x, and then individual neurons were located within the slice at 60x (excitation, 540 nm: emission, 605 nm). Imaging was performed with a Hamamatsu ORCA Flash 4.0LT sCMOS Camera (Hamamatsu Photonics, Japan). Identified neurons were approached with the whole-cell patch pipette controlled by a Sutter Instruments micromanipulator system, which was equipped with a MP-285 micromanipulator and a MPC-200 controller (Sutter Instruments, CA, USA). A P87 horizontal pipette puller (Sutter Instruments, Novato, CA, USA) was used to pull patch pipette, which had resistances of 2-3 MΩ when filled with solution containing the follow composition (in mM): 110 K-

gluconate, 2 $MgCl_2$, 10 HEPES, 1 Na_2-ATP, 0.1 Na_2-GTP, 2.5 EGTA. The cell of interest was approached with gentle positive pressure on the pipette. When an indentation could be seen on the cell in the bright field with IR-DIC optics, positive pressure was removed and a >1 GΩ was formed by applying slight negative pressure through the pipette by mouth. Whole-cell access was obtained by rapid negative pressure applied by mouth to rupture the GΩ seal. For measurements of excitatory postsynaptic currents, cells were voltage clamped at -80 mV to record synaptic currents mediated by AMPA receptors (5). When spontaneous excitatory synaptic currents (sEPSCs) were recorded in aCSF, no TTX was included during the recording. When miniature excitatory postsynaptic currents (mESPCs) were recorded, 500 nM TTX was added the aCSF. A +10 mV step was periodically performed to estimate series resistance (peak of the transient current) and input resistance (steady-state current) using Ohm's law. Measurements of membrane potential were made in current clamp, and firing rate was assessed at 3X rheobase in some current clamp prior to the application of TTX to measure mEPSCs. We often recorded more than one neuron per slice; however, TTX does not have a fast washout time in this preparation; therefore, firing properties in current clamp were not assessed for every cell. Previous work in these neurons suggests that firing response to current injection does not change in these neurons following hibernation (5), and our results in this study, despite a smaller sample size, support this previous finding.

Experimental Treatments

Three main series of experiments were performed in this study: (1) those that varied the duration of cold acclimation and then assessed synaptic function immediately after

removing the animal from the hibernation environment (Supplemental Fig. 1), (2) those that used either warm-acclimated control animals or 1 month hibernation animals and then exposed these brainstem preparations to TTX for 16 hrs in vitro (Fig 1-2 Supplemental Fig. 2-4), and (3) those that used either warm-acclimated control animals or 1 month hibernation animals and exposed each to 10 µM nimodipine for 16 hrs (Fig 3-4). For series 1 experiments control frogs (20°C) or cold-acclimated (2°C for 2 or 4 weeks) were used, and then synaptic function was assessed after animals were removed from these environments to roughly determine the time course of synaptic compensation. In series two experiments our main goal was to compare to post-hibernation synaptic function to acute inactivity with 100 nM TTX. In addition, we assessed synaptic function in post-hibernation animals after silencing rhythmic motor output with TTX. TTX silenced all preparations for the entire 16 hr period (data not shown). In series three experiments, we exposed warm-acclimated control and post-hibernation rhythmic preparations to 10 µM nimodipine for 16 hrs to block L-type Ca^{2+} channels in frog respiratory motoneurons (32), and a separate time control group was run in parallel. Following these treatments all synaptic recordings were performed in standard aCSF with 500 nM TTX. For Fig. 4, extracellular output from the cut vagus nerve via a bipolar suction electrode connected to an A-M Systems Model 1700 amplifier (bandpass filtered between 10-1000 Hz, 100X gain). Activity of this nerve is primarily generated by the 4th branch of the vagus nerve (the same neurons we studied in slices), and provides the main drive to the glottal dilator, which gates airflow into and out of the lung in anuran amphibians (52).

Data Analysis

All data analysis was performed using the peak analysis module on LabChart 8 (ADInstruments, Sydney, Australia). sEPSC and mESPCs events were recorded for 30 seconds and averaged to estimate excitatory synaptic drive due to AMPAR transmission. Cutoff amplitude was set at 7 pA. All analysis files were checked by eye to verify EPSCs were correctly identified. To infer synaptic scaling, a series of 50 mESPCs were chosen for each cell in the group and the entire distribution was ranked from lowest to highest for control and treatment conditions. In some cases, control and treatment conditions had different numbers of cells. In these situations, cells were randomly removed for the scaling analysis by assigning a number to each cell and then using a random number generator chose which cell(s) would be removed. This allowed equal number of mESPCs to be ranked and scaled in each group. Ranked data were plotted and then fit by a linear regression to obtain the slope of the line and intercept for the entire population. ~5-10 mEPSC events in each group showed extreme values that deviated from the line. These events may be caused by activation of subsaturated AMPA receptors, as suggested previously (23) and were therefore removed for the fitting of the ranked data. Each mESPC event in the treatment distribution was then mathematically downscaled by the equation of the fit from the linear regression and plotted as cumulative distributions. Input and series resistances were calculated by making a 10 mV step, from -80 mV to -70 mV. Series resistance did not vary across groups, and cells with series resistance of >25MΩ were discarded.

Statistics:

Data were analyzed and plotted using GraphPad Prism. Comparisons between two groups were made using a two-tailed unpaired t test. When standard deviations were

different between groups, a Welch's test was applied. Analyses involving three or more groups were performed using a one-way ANOVA and followed by Holm-Sidak's multiple comparisons test. When comparing two cumulative distributions, the Kolmogorov Smirnov test was run. To infer synaptic scaling, a series of 50 mESPCs were chosen per cell and then assessed using the rank-order method of the original synaptic scaling study (13). When comparing two cumulative distributions, the Kolmogorov Smirnov test was run. Significance was accepted at $p<0.05$.

Acknowledgements: This research funded in part by the Department of Defense (W911NF2010275), the National Institutes of Health (1R01NS114514 and 1R15NS112920), and lab startup funds from UNC-Greensboro to J.M.S.

Competing Interests: The authors declare no competing interests.

References:

1. Marder E & Goaillard J-M (2006) Variability, compensation and homeostasis in neuron and network function. *Nature Reviews Neuroscience* 7(7):563-574.
2. Desai NS, Cudmore RH, Nelson SB, & Turrigiano GG (2002) Critical periods for experience-dependent synaptic scaling in visual cortex. *Nature neuroscience* 5(8):783-789.
3. Pratt KG & Aizenman CD (2007) Homeostatic regulation of intrinsic excitability and synaptic transmission in a developing visual circuit. *Journal of Neuroscience* 27(31):8268-8277.
4. Diering GH*, et al.* (2017) Homer1a drives homeostatic scaling-down of excitatory synapses during sleep. *Science* 355(6324):511-515.
5. Santin JM, Vallejo M, & Hartzler LK (2017) Synaptic up-scaling preserves motor circuit output after chronic, natural inactivity. *eLife* 6.
6. Wu C-H, Ramos R, Katz DB, & Turrigiano GG (2021) Homeostatic synaptic scaling establishes the specificity of an associative memory. *Current Biology*.
7. Dickman D & Wondolowski J (2013) Emerging links between homeostatic synaptic plasticity and neurological disease. *Frontiers in cellular neuroscience* 7:223.
8. Styr B & Slutsky I (2018) Imbalance between firing homeostasis and synaptic plasticity drives early-phase Alzheimer's disease. *Nature neuroscience*:1.
9. Wolfart J & Laker D (2015) Homeostasis or channelopathy? Acquired cell type-specific ion channel changes in temporal lobe epilepsy and their antiepileptic potential. *Frontiers in physiology* 6:168.
10. Ren Z*, et al.* (2016) Bidirectional homeostatic regulation of a depression-related brain state by gamma-aminobutyric acidergic deficits and ketamine treatment. *Biological psychiatry* 80(6):457-468.
11. Davis GW (2013) Homeostatic signaling and the stabilization of neural function. *Neuron* 80(3):718-728.
12. Turrigiano G (2011) Too many cooks? Intrinsic and synaptic homeostatic mechanisms in cortical circuit refinement. *Annual review of neuroscience* 34:89-103.
13. Turrigiano GG, Leslie KR, Desai NS, Rutherford LC, & Nelson SB (1998) Activity-dependent scaling of quantal amplitude in neocortical neurons. *Nature* 391(6670):892-896.
14. Gainey MA, Hurvitz-Wolff JR, Lambo ME, & Turrigiano GG (2009) Synaptic scaling requires the GluR2 subunit of the AMPA receptor. *Journal of Neuroscience* 29(20):6479-6489.
15. Gainey MA, Tatavarty V, Nahmani M, Lin H, & Turrigiano GG (2015) Activity-dependent synaptic GRIP1 accumulation drives synaptic scaling up in response to action potential blockade. *Proceedings of the National Academy of Sciences* 112(27):E3590-E3599.
16. Lambo ME & Turrigiano GG (2013) Synaptic and intrinsic homeostatic mechanisms cooperate to increase L2/3 pyramidal neuron excitability during a late phase of critical period plasticity. *Journal of Neuroscience* 33(20):8810-8819.

17. Thiagarajan TC, Lindskog M, & Tsien RW (2005) Adaptation to synaptic inactivity in hippocampal neurons. *Neuron* 47(5):725-737.
18. Hanes AL*, et al.* (2020) Divergent synaptic scaling of miniature epscs following activity blockade in dissociated neuronal cultures. *Journal of Neuroscience* 40(21):4090-4102.
19. Echegoyen J, Neu A, Graber KD, & Soltesz I (2007) Homeostatic plasticity studied using in vivo hippocampal activity-blockade: synaptic scaling, intrinsic plasticity and age-dependence. *PloS one* 2(8):e700.
20. Lee KJ*, et al.* (2013) Mossy fiber-CA3 synapses mediate homeostatic plasticity in mature hippocampal neurons. *Neuron* 77(1):99-114.
21. Barnes SJ*, et al.* (2017) Deprivation-induced homeostatic spine scaling in vivo is localized to dendritic branches that have undergone recent spine loss. *Neuron* 96(4):871-882. e875.
22. Turrigiano G (2012) Homeostatic synaptic plasticity: local and global mechanisms for stabilizing neuronal function. *Cold Spring Harbor perspectives in biology* 4(1):a005736.
23. Kim J & Tsien RW (2008) Synapse-specific adaptations to inactivity in hippocampal circuits achieve homeostatic gain control while dampening network reverberation. *Neuron* 58(6):925-937.
24. Santin JM (2019) Motor inactivity in hibernating frogs: Linking plasticity that stabilizes neuronal function to behavior in the natural environment. *Developmental neurobiology*. 79(9):880-891
25. Santin JM & Hartzler LK (2016) Control of lung ventilation following overwintering conditions in bullfrogs, Lithobates catesbeianus. *Journal of Experimental Biology*. 219(13):2003-14
26. Santin JM & Hartzler LK (2017) Activation of respiratory muscles does not occur during cold-submergence in bullfrogs, Lithobates catesbeianus. *Journal of Experimental Biology* 220(7):1181-1186.
27. Ibata K, Sun Q, & Turrigiano GG (2008) Rapid synaptic scaling induced by changes in postsynaptic firing. *Neuron* 57(6):819-826.
28. Fong M-f, Newman JP, Potter SM, & Wenner P (2015) Upward synaptic scaling is dependent on neurotransmission rather than spiking. *Nature communications* 6.
29. Kim J, Tsien RW, & Alger BE (2012) An improved test for detecting multiplicative homeostatic synaptic scaling. *PloS one* 7(5):e37364.
30. Pacheco AT, Bottorff J, Gao Y, & Turrigiano GG (2021) Sleep promotes downward firing rate homeostasis. *Neuron* 109(3):530-544. e536.
31. I Stanika R, E Flucher B, & J Obermair G (2015) Regulation of postsynaptic stability by the L-type calcium channel CaV1. 3 and its interaction with PDZ proteins. *Current molecular pharmacology* 8(1):95-101.
32. Bueschke N, Amaral-Silva Ld, Hu M, & Santin JM (2021) Lactate ions induce synaptic plasticity to enhance output from the central respiratory network. *The Journal of physiology*. 599.25: 5485–5504
33. Greer J, Smith J, & Feldman J (1991) Role of excitatory amino acids in the generation and transmission of respiratory drive in neonatal rat. *The Journal of physiology* 437(1):727-749.

34. Johnson SM, Wilkerson JE, Wenninger MR, Henderson DR, & Mitchell GS (2002) Role of synaptic inhibition in turtle respiratory rhythm generation. *The Journal of physiology* 544(1):253-265.
35. Pekala D & Wenner P (2021) The uniform and non-uniform nature of slow and rapid scaling in embryonic motoneurons. *The Journal of Neuroscience: the Official Journal of the Society for Neuroscience*. In press.
36. Golowasch J, Goldman MS, Abbott L, & Marder E (2002) Failure of averaging in the construction of a conductance-based neuron model. *Journal of neurophysiology* 87(2):1129-1131.
37. Prinz AA, Bucher D, & Marder E (2004) Similar network activity from disparate circuit parameters. *Nature neuroscience* 7(12):1345-1352.
38. Louros SR, Hooks BM, Litvina L, Carvalho AL, & Chen C (2014) A role for stargazin in experience-dependent plasticity. *Cell reports* 7(5):1614-1625.
39. Wang G, Zhong J, Guttieres D, & Man H-Y (2019) Non-scaling regulation of AMPA receptors in homeostatic synaptic plasticity. *Neuropharmacology* 158:107700.
40. Blackman MP, Djukic B, Nelson SB, & Turrigiano GG (2012) A critical and cell-autonomous role for MeCP2 in synaptic scaling up. *Journal of Neuroscience* 32(39):13529-13536.
41. Joseph A & Turrigiano GG (2017) All for one but not one for all: Excitatory synaptic scaling and intrinsic excitability are coregulated by CaMKIV, while inhibitory synaptic scaling is under independent control. *Journal of Neuroscience*:0618-0617.
42. Wang H-L, Zhang Z, Hintze M, & Chen L (2011) Decrease in calcium concentration triggers neuronal retinoic acid synthesis during homeostatic synaptic plasticity. *Journal of Neuroscience* 31(49):17764-17771.
43. Li Y, Gorassini MA, & Bennett DJ (2004) Role of persistent sodium and calcium currents in motoneuron firing and spasticity in chronic spinal rats. *Journal of neurophysiology* 91(2):767-783.
44. Li B*, et al.* (2020) Neuronal Inactivity Co-opts LTP Machinery to Drive Potassium Channel Splicing and Homeostatic Spike Widening. *Cell*.
45. Santin J & Hartzler L (2013) Temperature influences CO_2/pH-sensitivity in locus coeruleus neurons of the bullfrog, *Lithobates catesbeianus*. *FASEB J* 27(714.12).
46. Santin J & Hartzler L (2015) Activation state of the hyperpolarization-activated current (Ih) modulates temperature-sensitivity of firing in locus coeruleus neurons from bullfrogs. *American journal of physiology. Regulatory, integrative and comparative physiology* 308:R1045-R1061.
47. Sanders CE & Milsom WK (2001) The effects of tonic lung inflation on ventilation in the American bullfrog Rana catesbeiana Shaw. *Journal of Experimental Biology* 204(15):2647-2656.
48. Schmidt RS (1965) Larynx control and call production in frogs. *Copeia*:143-147.
49. Bülow P, Murphy T, Bassell GJ, & Wenner P (2019) Homeostatic intrinsic plasticity is functionally altered in Fmr1 KO cortical neurons. *Cell reports* 26(6):1378-1388. e1373.

50. Soden ME & Chen L (2010) Fragile X protein FMRP is required for homeostatic plasticity and regulation of synaptic strength by retinoic acid. *Journal of Neuroscience* 30(50):16910-16921.
51. Zhong X, Li H, & Chang Q (2012) MeCP2 phosphorylation is required for modulating synaptic scaling through mGluR5. *Journal of Neuroscience* 32(37):12841-12847.
52. Sakakibara Y (1983) The pattern of respiratory nerve activity in the bullfrog. *The Japanese journal of physiology* 34(2):269-282.

Figures and Legends

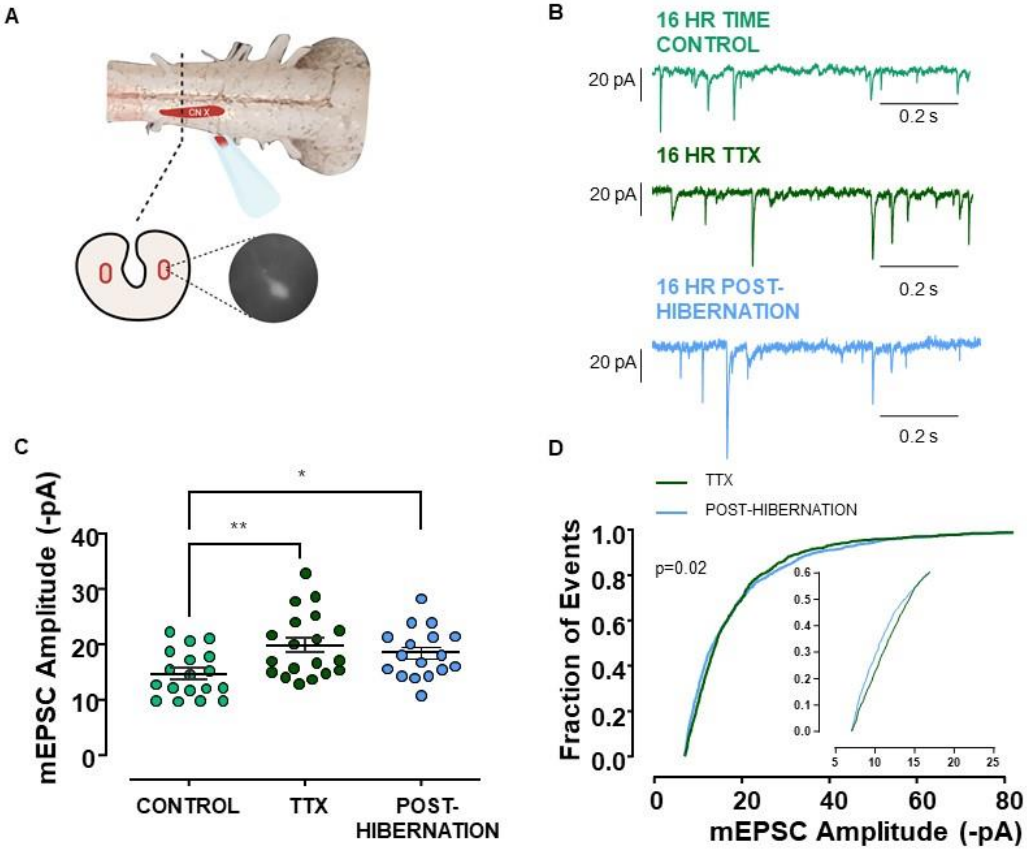

Figure 1 Hibernation and TTX both induce increases in mEPSC amplitude through different distributions. (A) Schematic of the experimental process to label respiratory motoneurons. The 4th root of the vagus nerve was backfilled with fluorescent dextran, and neurons were identified in slices through fluorescence imaging microscopy. (B) Example mEPSC traces recorded in whole-cell voltage clamp in laryngeal motoneurons in time control, TTX, and following hibernation. (C) Mean data showing enhanced mEPSC amplitude following both hibernation and TTX exposure relative to time control (One-way ANOVA, Holm-Sidak Multiple Comparisons Test, control vs. TTX, $p=0.004$, control vs. post-hibernation, $p=0.0139$, TTX vs. post-hibernation, $p=0.4405$). Circles represent cell-averaged mEPSCs for each neuron. Error bars are S.E.M. Horizontal line represents the mean. Control (n=18 from 5 animals), TTX (n=19 from 5 animals), post-hibernation (n=17 from 4 animals). (D) Hibernation and TTX produced slightly different distributions of individual mEPSCs (50 mEPSCs plotted per neuron; Kolmogorov-Smirnov Test). Curves represent the cumulative distribution of mEPSC amplitudes *$p<0.05$, **$p<0.01$.

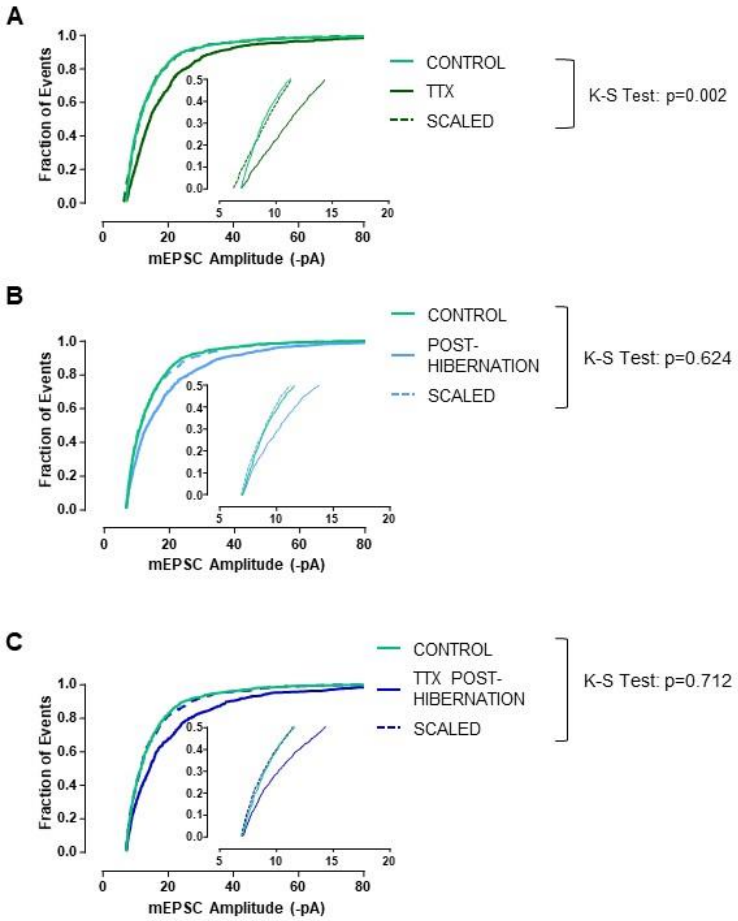

Figure 2 Hibernation, but not TTX, upregulates mESPC amplitudes through multiplicative synaptic scaling. (A-C) Cumulative distributions of mEPSC amplitudes for time control, treatment (TTX, post-hibernation, or post-hibernation+TTX), and mathematically downscaled treatment distributions. TTX does not lead to precise scaling of mEPSC amplitudes (A), and hibernation does regardless of whether activity is present (B) or absent (C) in the post-hibernation period. All comparisons between control and treatment yielded p values <0.0001 (Kolmogorov-Smirnov Test.). P values shown in the figures compare control vs. scaled distributions (Kolmogorov-Smirnov Test).

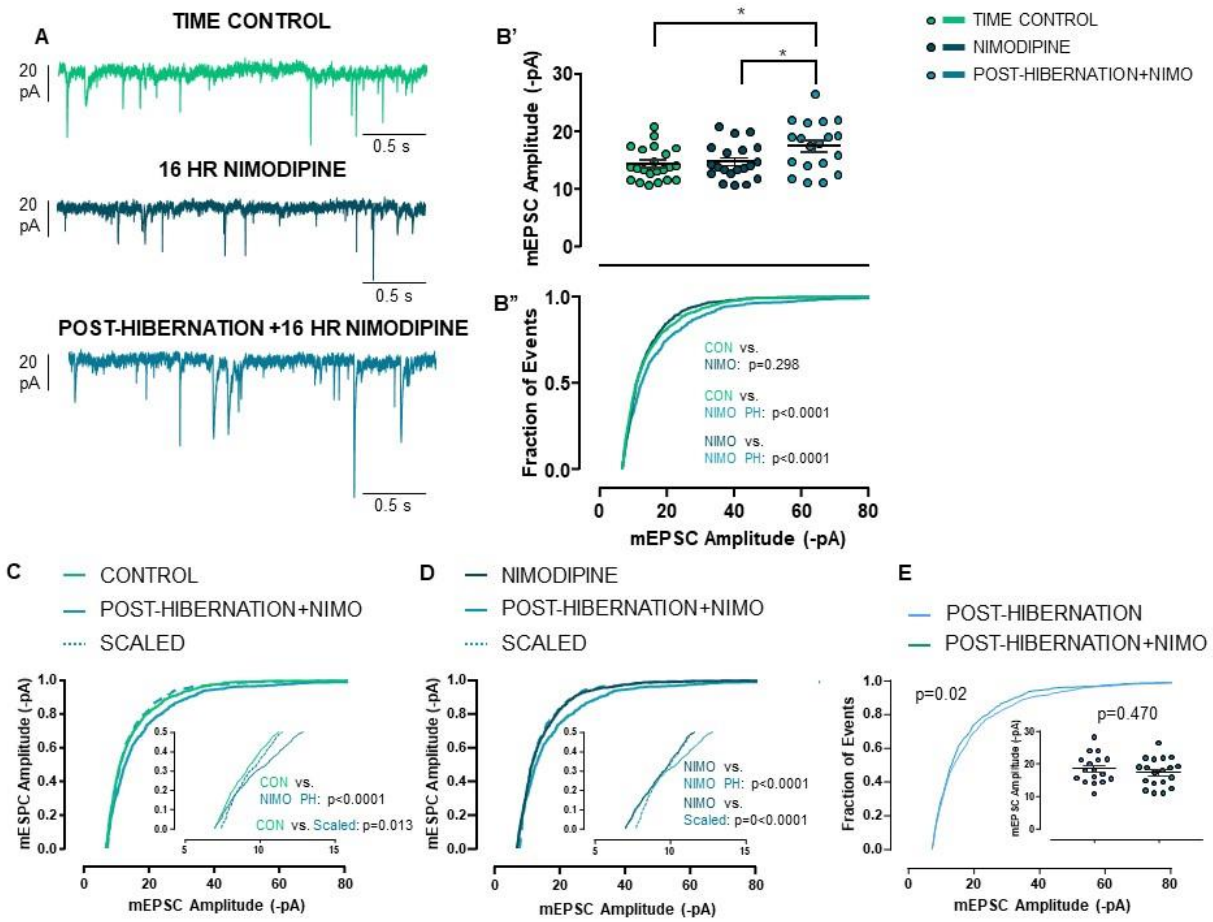

Figure 3 L-type Ca^{2+} channel signaling maintains multiplicative scaling after hibernation but not the increase in mean synaptic drive. (A) Example mEPSC traces recorded in whole-cell voltage clamp in time control (n=22 from 6 animals), 10 µM nimodipine (n=20 from 5 animals), and post-hibernation+nimodipine (n=19 from 5 animals). (B') Cell-averaged mEPSC amplitudes and (B'') cumulative distribution of mEPSC amplitudes (50 mEPSCs plotted per cell). Nimodipine exposure does not increase mean synaptic strength or alter the distribution of mEPSC amplitudes. After hibernation, exposure to nimodipine still results in enhanced synaptic strength. (C-D) Cumulative distributions showing the test for scaling after hibernation following nimodipine exposure. Nimodipine undoes multiplicative synaptic scaling following hibernation when compared using the time control distribution and nimodipine exposure in warm animals that did not undergo hibernation. (E) Post-hibernation (n=17 from 5 animals) and post-hibernation+ nimodipine (n=19) have similar group means (t test) but have significantly different distributions, owing to a left shift (weakening) in the upper 50% of the distribution (Kolmogorov-Smirnov Test).

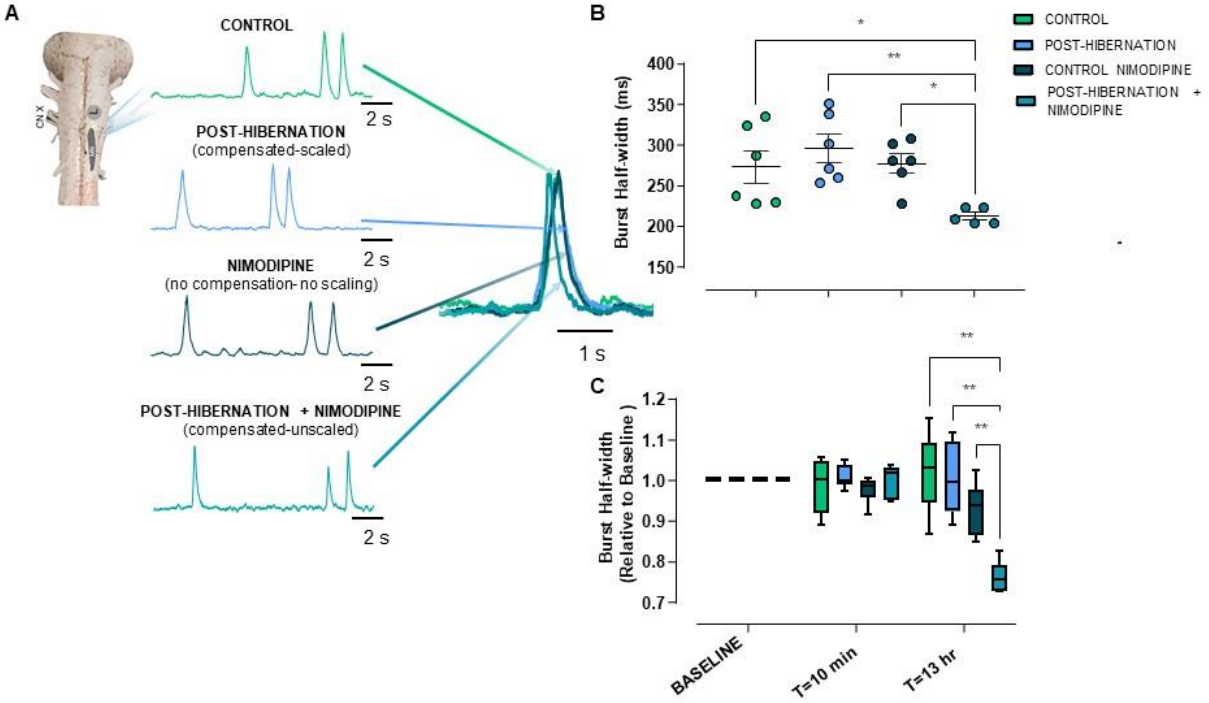

Figure 4 A failure to precisely scale motoneuron synaptic strength is associated with reduced respiratory motor outflow. (A) Simplified schematic of the brainstem preparation, highlighting integrated respiratory-related motor output recorded from the vagus nerve. The four groups shown are time control, post-hibernation (associated with scaled compensation), nimodipine in warm-acclimated control (no compensation, no scaling), and post-hibernation+nimodipine (unscaled compensation) for 13 hrs *in vitro*. Traces are compressed or expanded and overlayed to highlight differences across groups. (B) Nimodipine applied following hibernation resulted in narrower respiratory bursts from the vagus nerve (One-way ANOVA with Holm-Sidak's Multiple Comparisons Test; control vs. post-hibernation nimo, p=0.049, post-hibernation vs. posthibernation nimo, p=0.007, nimo vs posthibernation nimo=0.041). (C) Nimodipine resulted in a slow, reduction of burst width specific to the post-hibernation group, as acute exposure to nimodipine did not affect burst amplitude in any group (Two-way ANOVA followed by Holm-Sidak's multiple comparisons test). n= 6,6,6, and 5 brainstem preparations for control, post-hibernation, nimodipine, and post-hibernation nimodipine, respectively. *p<0.05, **p<0.01.

Figure Supplements: A requirement for correctly scaled synapses in the regulation of motor circuit output

Supplemental Figures

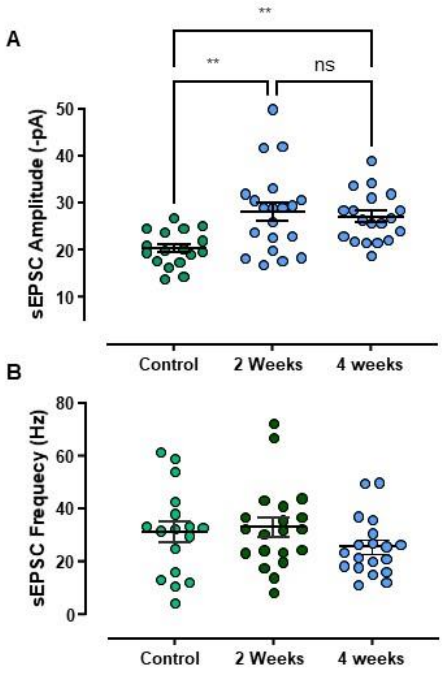

Figure S1 sEPSC amplitude, but not frequency, increases by two weeks of cold-acclimation. Animals were either warm-acclimated (control; 22°C; n=17), or cold-acclimated for two (n=20) or four weeks (n=19). (A) sEPSC amplitude but not frequency (B) was increased by 2 weeks and remained elevated at four weeks. Dots represent average values for individual neurons. Error bars or S.EM.

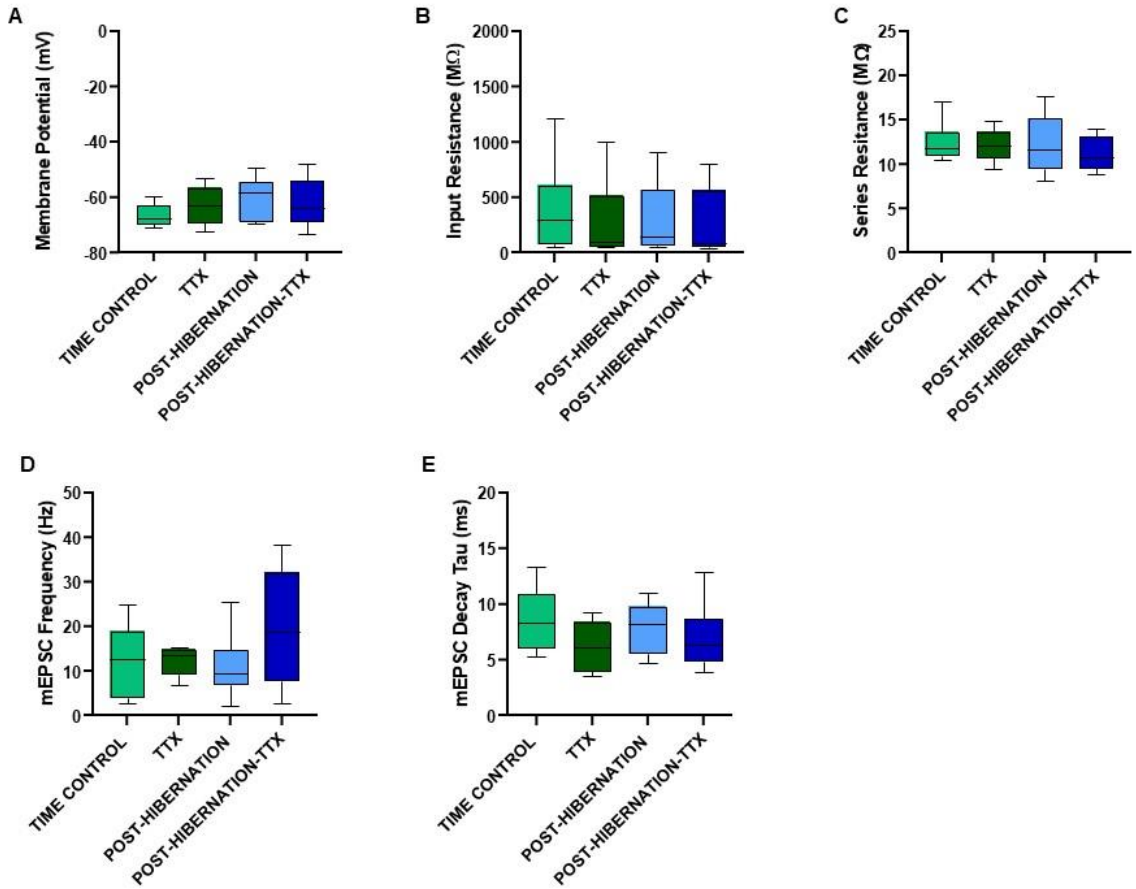

Figure S2 Membrane and other mEPSC properties are not affected following hibernation with or without activity in the post-hibernation period. (A-E) All variables were compared using a one-way ANOVA. No statistical difference was detected among treatments. Control (n=18), TTX (n=19), post-hibernation (n=17), post-hibernation+TTX (n=16). Box and whisker plots show the interquartile range. Whiskers extend to maximum and minimum values.

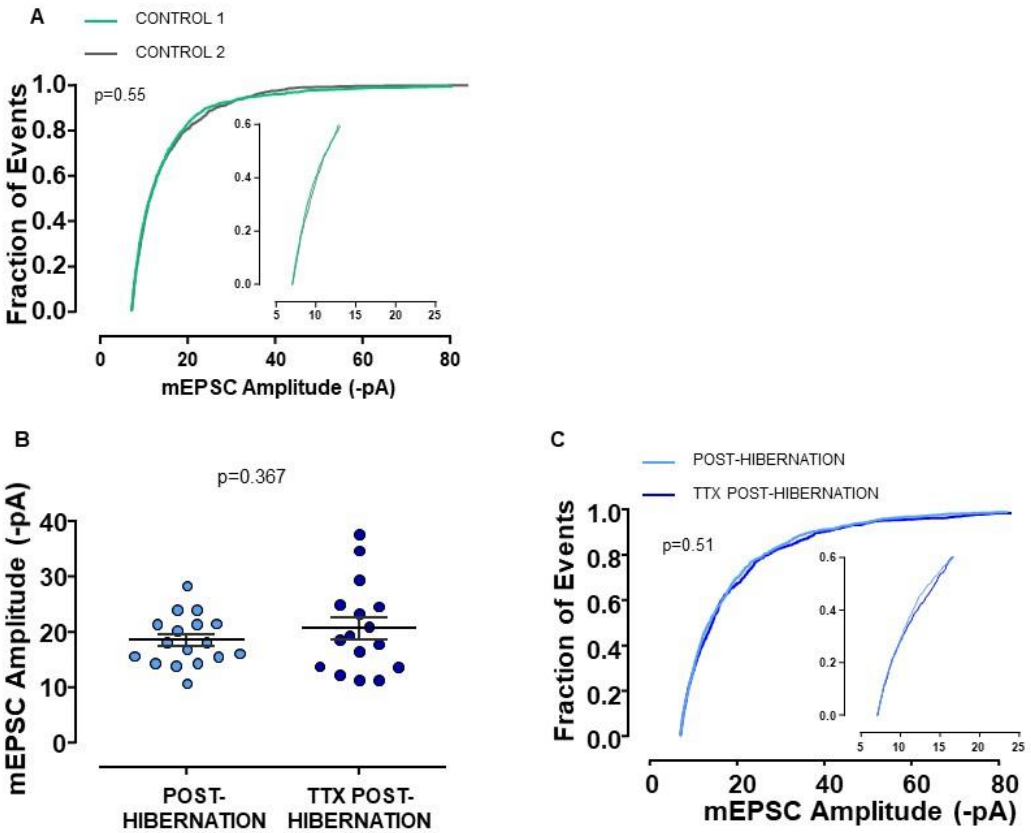

Figure S3 mEPSC distributions are stable and repeatable. (A) To determine variability in mEPSC distributions two time control groups were evaluated. Statistically indistinguishable distributions were observed between two control groups (Kolmogorov-Smirnov Test). Control 1=18 cells with 50 mEPSCs per cell and Control 2=19 cells with 50 mEPSCs per cell. (B-C) TTX in the post-hibernation period (n=16) do not affect cell-averaged mEPSC and mEPSC distributions compared to post-hibernation alone (n=17).

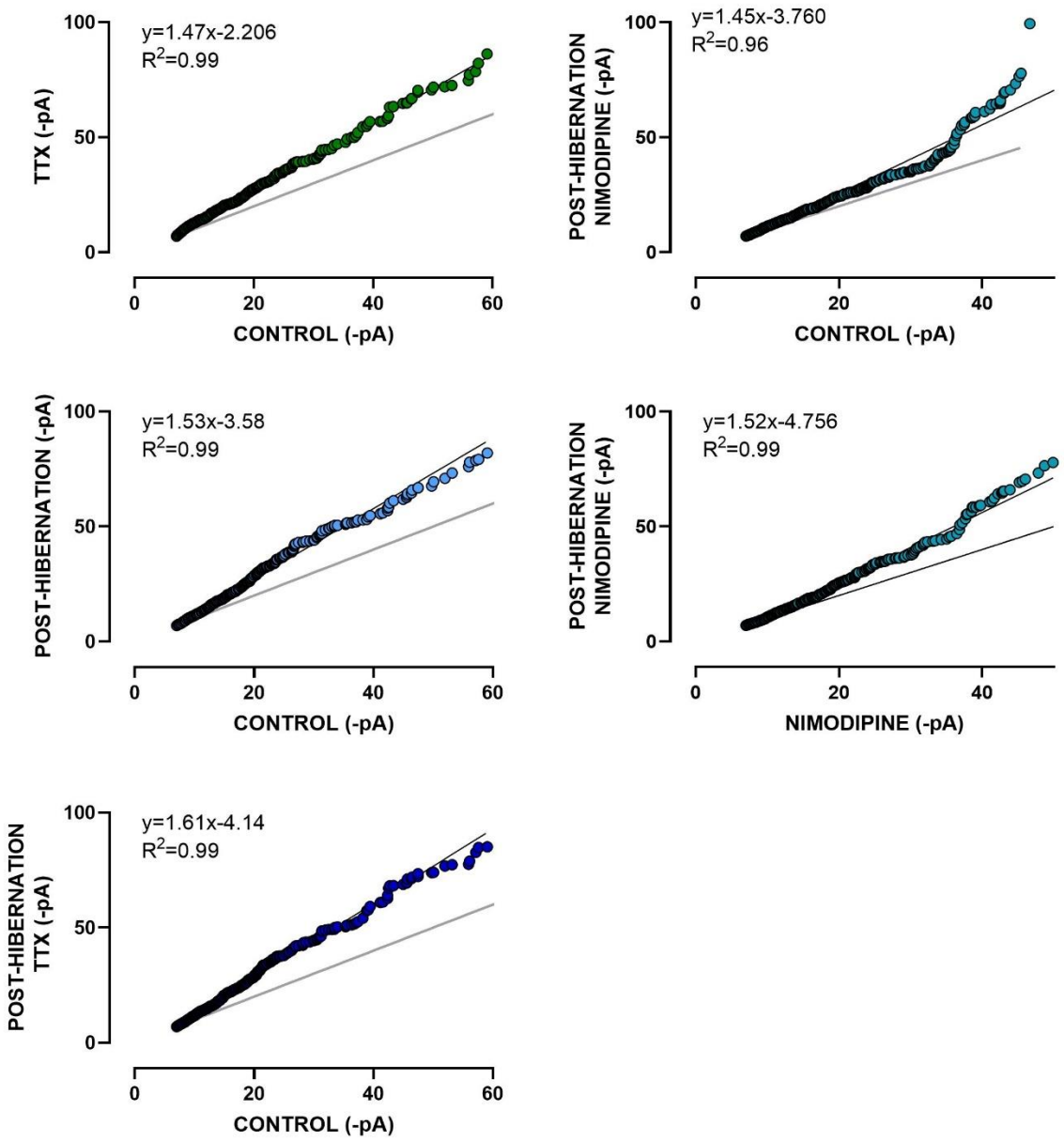

Figure S4 Rank order plots for all groups for determination of scaling factor in all experiments. 50 mEPSCs per cell were ranked for control and all treatment distributions, plotted against each other, and fit with a linear regression. The equation was used to mathematically downscale treatment distributions to test for scaling. Grey line in each plot shows the unity line.

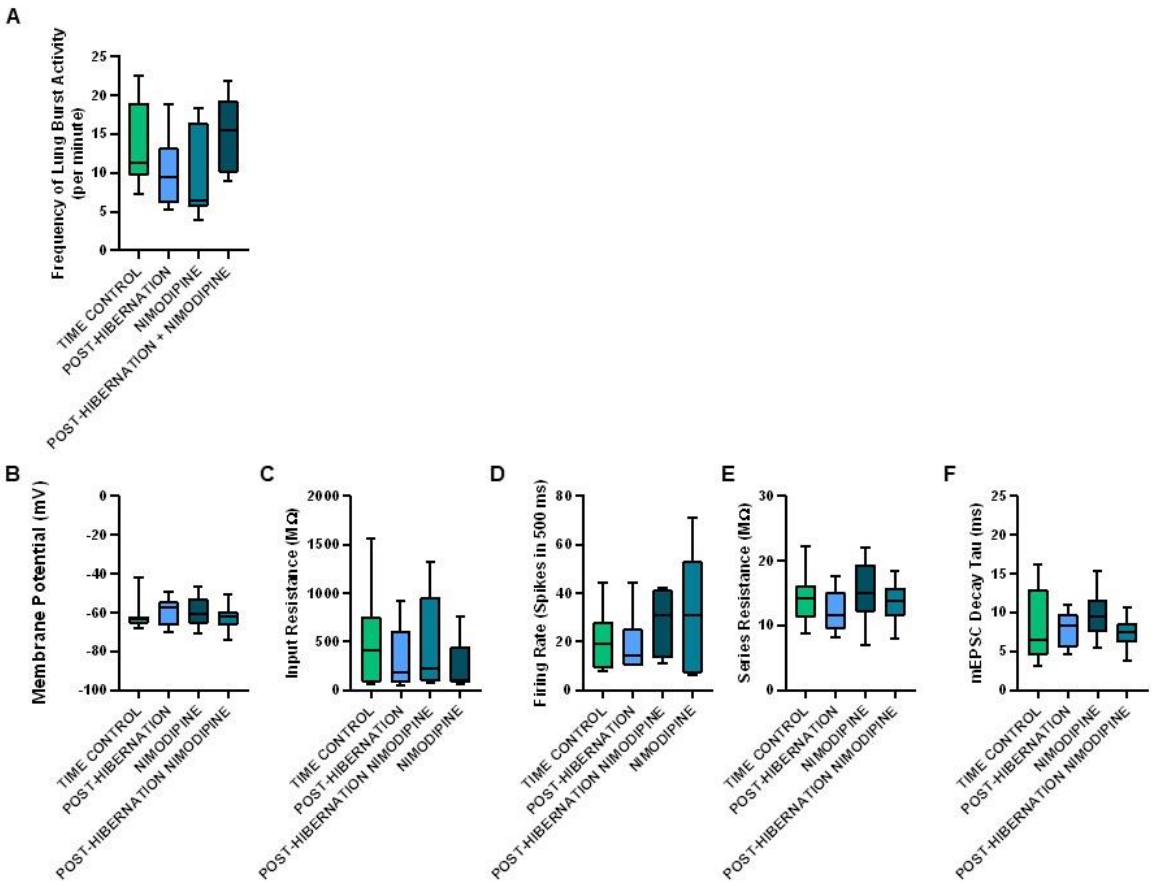

Figure S5 Narrow respiratory bursts following "unscaling" is not associated with changes population motor burst frequency (A), membrane potential (B), input resistance (C), firing frequency (at 3X rheobase; D), series resistance (E), and mEPSC decay tau (F). For (A), n= 6,6,6, and 5 brainstem preparations for control, post-hibernation, nimodipine, and post-hibernation nimodipine, respectively. For (B-C,E-F), n= 20, 17, 20, and 19 neurons for control, post-hibernation, nimodipine, and post-hibernation+nimodpine, respectively. For assessment of firing rate (D), n= 7,6,6,7 neurons were used in control, post-hibernation, nimodipine, and post-hibernation+nimodpine, respectively. Box and whisker plots show the interquartile range. Whiskers extend to maximum and minimum values.